Origin of planar Hall effect in type-II Weyl semimetal $MoTe_2$

Cite as: AIP Advances **9**, 055015 (2019); https://doi.org/10.1063/1.5094231
Submitted: 28 February 2019 • Accepted: 09 May 2019 • Published Online: 17 May 2019

D. D. Liang, Y. J. Wang, W. L. Zhen, et al.

Origin of planar Hall effect in type-II Weyl semimetal $MoTe_2$

Cite as: AIP Advances 9, 055015 (2019); doi: 10.1063/1.5094231
Submitted: 28 February 2019 • Accepted: 9 May 2019 •
Published Online: 17 May 2019

D. D. Liang,[1,2,a)] Y. J. Wang,[1,a)] W. L. Zhen,[1,a)] J. Yang,[1] S. R. Weng,[1] X. Yan,[1] Y. Y. Han,[1] W. Tong,[1] W. K. Zhu,[1,b)] L. Pi,[1,2,b)] and C. J. Zhang[1,3,b)]

AFFILIATIONS

[1]Anhui Province Key Laboratory of Condensed Matter Physics at Extreme Conditions, High Magnetic Field Laboratory, Chinese Academy of Sciences, Hefei 230031, China
[2]Hefei National Laboratory for Physical Sciences at Microscale, University of Science and Technology of China, Hefei 230026, China
[3]Institute of Physical Science and Information Technology, Anhui University, Hefei 230601, China

[a)]**Contributions:** D. D. Liang, Y. J. Wang and W. L. Zhen contributed equally to this work.
[b)]**Electronic addresses:** wkzhu@hmfl.ac.cn, pili@ustc.edu.cn, and zhangcj@hmfl.ac.cn.

ABSTRACT

Besides the negative longitudinal magnetoresistance (MR), planar Hall effect (PHE) is a newly emerging experimental tool to test the chiral anomaly or nontrivial Berry curvature in Weyl semimetals (WSMs). However, the origins of PHE in various systems are not fully distinguished and understood. Here we perform a systematic study on the PHE and anisotropic MR (AMR) of T_d-$MoTe_2$, a type-II WSM. Although the PHE and AMR curves can be well fitted by the theoretical formulas, we demonstrate that the anisotropic resistivity arises from the orbital MR (OMR), instead of the negative MR as expected in the chiral anomaly effect. In contrast, the positive MR indicates that the large OMR dominates over the chiral anomaly effect. This explains why it is difficult to measure negative MR in type-II WSMs. We argue that the measured PHE can be related with the chiral anomaly only when the negative MR is simultaneously observed.

I. INTRODUCTION

Weyl fermions in condensed matter systems represent the linearly dispersing low-energy excitations that obey a two-component Dirac equation.[1] Different from the type-I Weyl semimetals (WSMs, materials hosting Weyl fermions) which have standard Weyl points with a point-like Fermi surface, the type-II WSMs possess tilted Weyl points, arising at the contact of electron and hole pockets.[2] The orthorhombic phase (T_d) of layered transition metal dichalcogenides WTe_2 and $MoTe_2$ are theoretically predicted as the potential candidates for the type-II WSMs.[2,3] Signatures of Fermi arcs, the surface state of WSMs, have been indeed observed in the angle-resolved photoemission spectroscopy (ARPES) measurements for WTe_2[4,5] and $MoTe_2$.[6,7]

In transport experiments, WSMs are usually featured for the negative longitudinal magnetoresistance (NLMR) induced by chiral anomaly,[8,9] which refers to the non-conservation of chiral charge around the Weyl nodes when the applied electric and magnetic fields are non-orthogonal ($\boldsymbol{E}\cdot\boldsymbol{B} \neq 0$). The experimental measurement of NLMR is very critical, and especially for type-II WSMs, the NLMR can only be observed along specific crystalline directions and in samples with appropriate chemical potential (see Refs. 10 and 11 for the NLMR in WTe_2). Within our knowledge scope, so far, the NLMR has not been reported for $MoTe_2$. In the pure Weyl physics, the NLMR will induce non-zero off-diagonal components under the SO (3) rotation transformation, further leading to a planar Hall effect (PHE).[12,13] The chiral anomaly induced PHE (ρ_{yx}) and related anisotropic magnetoresistance (AMR, ρ_{xx}) can be expressed as[12]

$$\rho_{yx} = -\Delta\rho^{chiral}\sin\theta\cos\theta, \tag{1}$$

$$\rho_{xx} = \rho_{\perp} - \Delta\rho^{chiral}\cos^2\theta, \tag{2}$$

where θ is the angle of B with respect to current (I), $\Delta\rho^{chiral} = \rho_{\perp} - \rho_{\parallel}$ is the chiral anomaly induced anisotropic resistivity, $\rho_{\perp}$ and $\rho_{\parallel}$ are

the resistivity corresponding to $B \perp I$ and $B \parallel I$, respectively. Note that the chiral anomaly based NLMR and PHE are the same thing. All the effects that occur in the NLMR measurements will affect the PHE.

Since the theoretical proposals suggest that the chiral anomaly in topological semimetals can induce a PHE,[12,13] the PHE has been widely used to investigate the chiral anomaly in topological semimetals and candidates.[14–21] However, the origins of PHE in various systems are not fully distinguished and understood. More seriously, the observation of PHE is directly claimed equivalent to chiral anomaly in several researches,[20,21] without careful analysis about the origin of anisotropic resistivity. This suggests a misuse of such a measurement technique. Actually, PHE usually has other origins in various systems, including anisotropic magnetic scattering,[22,23] topological surface state,[24] and orbital magnetoresistance (OMR).[14] To clarify these confusions, it is necessary to test the PHE in a material that lacks the chiral anomaly induced NLMR. $MoTe_2$, a confirmed WSM, is such a material.

In this paper, we perform a systematic study on the PHE and AMR of T_d-$MoTe_2$, in which the NLMR induced by chiral anomaly is not observed. Although the PHE and AMR curves can be well fitted by the theoretical formulas, we demonstrate that the anisotropic resistivity $\Delta\rho$ arises from the OMR that increases the $\rho_\perp$ more quickly, instead of the reduced $\rho_\parallel$ as expected in the chiral anomaly effect, which is distinctly different from Ref. 20. In contrast, the positive LMR indicates that the large OMR dominates over the chiral anomaly effect. This explains why it is difficult to measure NLMR in type-II WSMs. We argue that the measured PHE can be related with chiral anomaly only when the NLMR is simultaneously observed.

II. EXPERIMENTAL METHODS

T_d-$MoTe_2$ single crystals were grown by a self-flux method (Te). Powders of Mo (Alfa Aesar, 99.9%) and Te (Alfa Aesar, 99.99%) were ground and placed into a quartz ampoule, then heated up to 1373 K. The ampoule was cooled down to 1223 K at a rate of 2 K/h. The excess Te flux was removed by centrifugation. Finally, long flake-like crystals were obtained [inset of Fig. 1(a)]. The crystal structure and phase purity were checked by single crystal X-ray diffraction (XRD) on a Rigaku-TTR3 X-ray diffractometer using Cu Kα radiation. The single crystals are exfoliated into a thin plate to perform the transport measurements, with dimensions of $4\times0.5\times0.2$ mm^3. All the electrical measurements were taken on a Quantum Design PPMS.

III. RESULTS AND DISCUSSION

Figure 1(a) presents the single crystal XRD pattern taken at room temperature, which is consistent with the *1T'* phase of $MoTe_2$.[25] Only the (00*l*) peaks are detected, suggesting that the naturally cleaved surface is the *ab* plane. Such a distorted octahedral phase will transit to an orthorhombic T_d phase at low temperature. This transition shows a signature in the resistivity measurement as a function of temperature, where a kink is observed at about 250 K [Fig. 1(b)].[26] A relatively large residual resistivity ratio, i.e., RRR = $\frac{\rho_{300K}}{\rho_{2K}}$ = 156, is further indicative of the high quality of the sample.

In order to obtain the carrier mobility and density, the (regular) Hall effect and magnetoresistance (MR) are measured on the *ab* plane, with the magnetic field applied along the *c* axis [inset of Fig. 1(c)]. As shown in Fig. 1(c), the linear magnetic field dependence of ρ_{xy} suggests a nearly electron-hole compensated situation.[25] Figure 1(d) shows the MR curve taken at 2 K, as well as the power law fit. The resultant component of n=1.87 is consistent with the nearly compensated situation (n=2 for perfect compensation). Assuming $n_e = n_h$ in a two-band model,[27] the MR ratio $\frac{\rho_{xx}(B)-\rho_{xx}(0)}{\rho_{xx}(0)}$ is equal to $\mu_e\mu_h B^2$, where n_e (n_h) and μ_e (μ_h) are the carrier density and mobility for electrons (holes), respectively. Using this formula to fit the MR

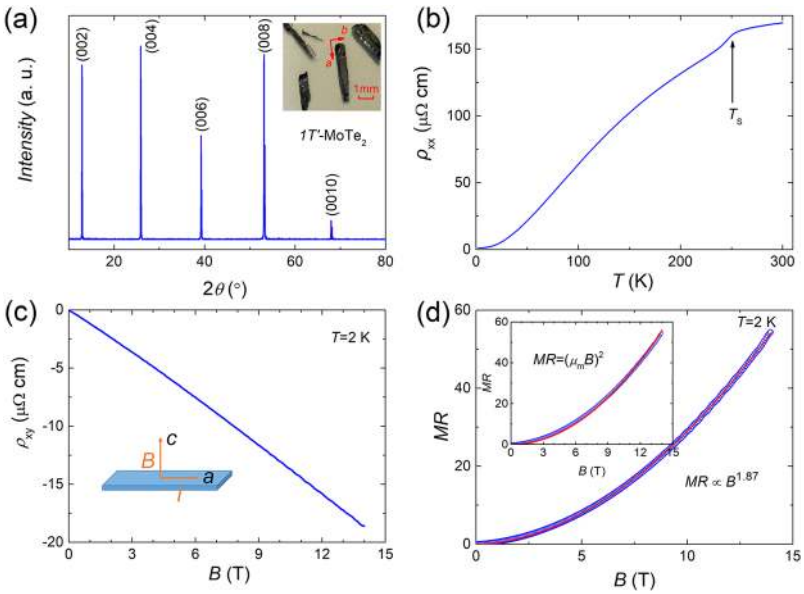

FIG. 1. (a) Single crystal XRD pattern taken at room temperature. Inset: image of as-grown single crystals. Red arrows indicate the crystalline axes. (b) ρ_{xx} as a function of temperature taken at zero magnetic field, showing a first order phase transition at ~250 K. (c) Regular Hall resistivity ρ_{xy} taken at 2 K in a magnetic field up to 14 T. Inset: the configuration of *B* and *I* for Hall effect and MR measurements. (d) MR ratio taken at 2 K in a magnetic field up to 14 T. Red solid curve represents the power law fit using the formula $MR = aB^n$. Inset: MR and the fitting curve using $MR = (\mu_m B)^2$.

curve yields a geometric-mean mobility $\mu_m = \sqrt{\mu_e \mu_h}$=5300 cm^2/Vs [inset of Fig. 1(d)]. This value is not as ultrahigh as in Cd_3As_2 (~10^6 cm^2/Vs)[28] or TaAs (~10^5 cm^2/Vs),[29] but almost that of Na_3Bi and GdPtBi (3000 and 2000 cm^2/Vs at 2 K, respectively).[16] Such a relatively low mobility will lead to a large onset field B_c (inversely proportional to mobility) of current jetting. The B_c of Na_3Bi and GdPtBi can reach as high as 30 T.[16] Therefore, the current jetting is unlikely to be observed in the following PHE measurements for $MoTe_2$ (not more than 14 T). This is different from the case in TaP which has an ultrahigh mobility and enhanced current jetting.[19]

The measurement geometry of PHE and AMR is illustrated in Fig. 2(a). The standard four-probe technique is adopted to measure the LMR (ρ_{xx}) along the *a* axis, together with two Hall contacts to measure the planar Hall resistivity (ρ_{yx}). Magnetic field is applied within the *ab* plane and rotates around the *c* axis, with an angle θ relative to *I*. Two types of misalignment may exist in actual experimental set-up.[19] Type I is that the magnetic field does not always perfectly lie in the sample plane. Type II is the possible nonsymmetrical Hall contacts that will induce a small LMR (even function of θ) in the measured ρ_{yx}. Figure 2(b) shows the raw data of the angle-dependent ρ_{yx} taken at 2 K and 5 T. We can see a slight mismatch between the Hall data taken at θ and $\theta + \pi$. That is, for the magnetic fields *B* and $-B$, the major part of ρ_{yx} is even and the minor part is odd. The odd-in-*B* part satisfies the antisymmetry requirement of a true Hall effect, which is ascribed to the type-I misalignment, while the even-in-*B* part violates the antisymmetry property and is hence a pseudo Hall effect. To eliminate the regular Hall resistivity, we average the data of θ and $\theta + \pi$. The resultant curve ρ_{yx}^{PHE} shows an odd function feature in θ [Fig. 2(c)], suggesting that the type-II misalignment is negligible in our measurements.[19]

The angular dependence of ρ_{yx}^{PHE} has a period of π and reaches its maximums at $\pi/4$ and $3\pi/4$, both of which are consistent with the PHE. Using Eq. (1) to fit the experimental data results in an anisotropic resistivity $\Delta\rho$ = 2.28 uΩ cm. This value is comparable with that of $ZrTe_5$[18] and WTe_2,[17] but smaller than that of GdPtBi,[14,16] Na_3Bi[16] and TaP.[19] Figure 2(d) presents the angular dependence of ρ_{xx} taken at 2 K and 5 T. The type-I misalignment may induce a normal MR component in the measured ρ_{xx}. However, this effect can be also neglected if we note that the resultant $\Delta\rho$ from the AMR curve (2.15 uΩ cm) is consistent with the $\Delta\rho$ obtained from the PHE curve. The slight difference between them should arise from the sample dimensions used in the resistivity calculations.

The PHE measurements are further performed at different magnetic fields and temperatures, to test the magnetic field and temperature dependence of $\Delta\rho$. Figure 3(a) shows the angular dependence of ρ_{yx} taken at 2 K and various magnetic fields. The fittings to Eq. (1) give a series of $\Delta\rho$ for various *B*. As shown in Fig. 3(c), the magnetic field dependence of $\Delta\rho$ can be fitted to the power law with an exponent 1.5. In addition to magnetic field, temperature is another factor to influence the $\Delta\rho$, via changing the mobility. The relationship between mobility and the $\Delta\rho$ will be discussed in the next section. Figure 3(b) presents the angular dependence of ρ_{yx} taken at different temperatures and 14 T. The fitting results are plotted in Fig. 3(d), showing a remarkably decrease as temperature increases.

The anisotropic resistivity $\Delta\rho$ can be also revealed by the angular dependence measurement of longitudinal resistivity ρ_{xx}, viz., the AMR. Figure 4(a) shows the angle-dependent ρ_{xx} taken at 2 K and various magnetic fields. As magnetic field increases, the amplitude of ρ_{xx} rises quickly. The fittings using Eq. (2) result in a list of $\Delta\rho$, which can be further fitted to the power law curve ($\Delta\rho \propto B^{1.4}$) [Fig. 4(c)].

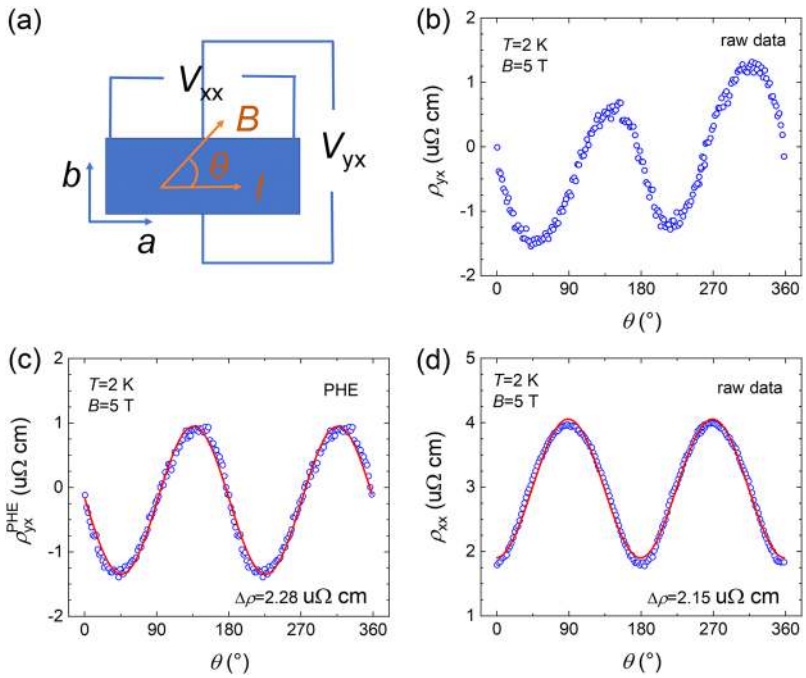

FIG. 2. (a) Schematic measurement geometry of PHE. (b) Raw data of the angle-dependent ρ_{yx} taken at 2 K and 5 T. (c) The obtained planar Hall resistivity ρ_{yx}^{PHE} after the averaging operation of θ and $\theta + \pi$. Red solid curve represents the fit to Eq. (1). (d) Raw data of the angle-dependent AMR ρ_{xx} taken at 2 K and 5 T. Red solid curve represents the fit to Eq. (2).

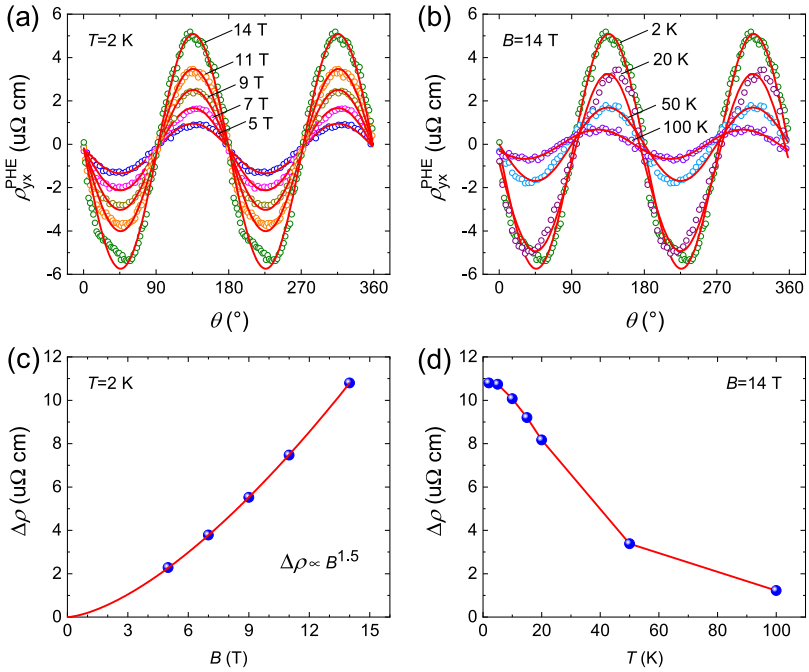

FIG. 3. Angular dependence of ρ_{yx}^{PHE} (a) taken at 2 K and various magnetic fields and (b) taken at various temperatures and 14 T. Red solid curves represent the fits to Eq. (1). (c) Magnetic field dependence of $\Delta\rho$, obtained from the fits in (a). Solid curve is a power law fit. (d) $\Delta\rho$ as a function of temperature, obtained from the fits in (b).

We note that the values of $\Delta\rho$ and the exponent obtained from the fitting are consistent with those in Fig. 3(c), again confirming the validity of our measurements and analyses.

To unveil the origin of $\Delta\rho$ that increases with B, the measured $\rho_\perp$ and $\rho_\parallel$ are extracted from the ρ_{xx} curves in Fig. 4(a). As seen in the inset of Fig. 4(c), the $\rho_\perp$ and $\rho_\parallel$ both increase as B increases. However, their behaviors are different. With the increasing B, the $\rho_\perp$ rises rapidly ($\rho_\perp \sim B^{1.45}$), while the $\rho_\parallel$ increases in a moderate way. Some important information could be retrieved from the inset figure. First, the natural extensions of $\rho_\perp$ and $\rho_\parallel$ intersect at one point on the y axis, i.e., ρ_0, the ρ_{xx} at zero magnetic field. This value is consistent with the ρ_{xx}-T measurement in Fig. 1(b). Second,

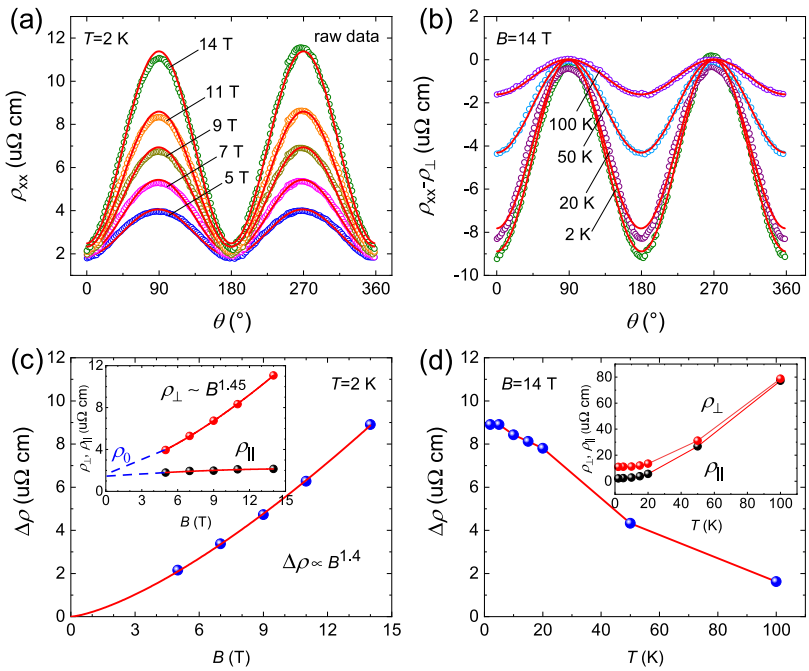

FIG. 4. (a) Raw data of the angle-dependent ρ_{xx} taken at 2 K and different magnetic fields. (b) Angular dependence of $\rho_{xx} - \rho_\perp$ taken at different temperatures and 14 T. Red solid curves represent the fits to Eq. (2). (c) Magnetic field dependence of $\Delta\rho$, obtained from the fits in (a). Solid curve is a power law fit. Inset: the $\rho_\perp$ and $\rho_\parallel$ extracted from the experimental data in (a). Solid curves represent the power law fit for $\rho_\perp$ and the 2nd order polynomial fit for $\rho_\parallel$, respectively. Blue dashed lines are their natural extensions. (d) $\Delta\rho$ as a function of temperature, obtained from the fits in (b). Inset: the $\rho_\perp$ and $\rho_\parallel$ extracted from the experimental data in (b).

the $\rho_{\parallel}$ shows a positive dependence on B, meaning that the LMR is positive. This is contrary to the expectation of an NLMR induced by the chiral anomaly. Although it is not concluded that the chiral anomaly does not exist in $MoTe_2$, it at least suggests that the chiral anomaly is dominated over by another factor that induces a positive LMR. Third, the main contribution of the increased $\Delta\rho$ ($=\rho_{\perp} - \rho_{\parallel}$) comes from the rapid increase of $\rho_{\perp}$, instead of the decrease of $\rho_{\parallel}$. We know that a nonzero $\Delta\rho$ can always produce a PHE curve, as is shown in Fig. 3(a). Therefore, the observation of PHE curves does not necessarily prove the existence of chiral anomaly. In this case, the PHE curves are associated with the excessively increased $\rho_{\perp}$.

Since the B-dependence of $\rho_{\perp}$ and $\rho_{\parallel}$ is far away from the quadratic dependence (n=1.87 in this case, see Fig. 1(d)), their increase with B is unlikely attributed to the addition of a normal MR due to the type-I misalignment. Taking account of the asymmetric Fermi surface of $MoTe_2$, the increase should arise from the OMR.[30] As suggested in Ref. 31, the OMR can significantly enhance the anisotropic conductivity $\Delta\sigma$ ($=\sigma_{\parallel} - \sigma_{\perp}$), and the B-dependence of $\Delta\sigma$ is completely the same with the chiral anomaly induced PHE. Therefore, it is difficult to distinguish the origin of the $\Delta\rho$ measured in PHE, unless the B-dependence of $\rho_{\perp}$ and $\rho_{\parallel}$ is also provided. As shown in the inset of Fig. 4(c), the OMR is highly anisotropic, increasing quickly for $\rho_{\perp}$ but slowly for $\rho_{\parallel}$. Hence, the existence of a large anisotropic OMR is the origin of PHE. Actually in the pure Weyl physics, the $\rho_{\perp}$ should be a constant, i.e., ρ_0. The increase of $\Delta\rho^{chiral}$ is mainly contributed by the decrease of $\rho_{\parallel}$, namely, the NLMR. For most cases, the NLMR is very small, because the ρ_0 of semimetals is usually small. For the present case, assuming that the chiral anomaly indeed exists and reduces the $\rho_{\parallel}$ to zero at a certain magnetic field, the largest contribution to $\Delta\rho$ is ρ_0 (~1.5 uΩ cm). However, this value is not sufficient to account for the large increase of $\Delta\rho$ (~8.9 uΩ cm at 14 T). The signature of chiral anomaly is fully covered by the OMR. This may explain why it is difficult to measure NLMR in $MoTe_2$.

We note that the authors of Ref. 20 connect the PHE in $MoTe_2$ with its chiral anomaly. However, we will see it is inappropriate, based on our additional data and analyses. Figure 4(b) shows the temperature dependence of $\rho_{xx} - \rho_{\perp}$ taken at various temperatures and 14 T. Consistent with the results in Fig. 3(d), the $\Delta\rho$ is greatly reduced when temperature increases [Fig. 4(d)]. The $\rho_{\perp}$ and $\rho_{\parallel}$, presented in the inset of Fig. 4(d), both increase with T (as in Fig. 1(b)), while their difference becomes smaller at a high T. That is, the enhanced thermal fluctuation reduces the resistivity anisotropy, even in the presence of an external magnetic field. The relationship between temperature (i.e., mobility) and the $\Delta\rho$ can be understood in the two-band model, where $\rho_{\perp} = \left[\frac{\sigma_e}{1+\mu_e^2B^2} + \frac{\sigma_h}{1+\mu_h^2B^2}\right]^{-1}$ and $\rho_{\parallel} = \left[\sigma_e + \sigma_h\right]^{-1}$.[16] $\sigma_e = n_e e\mu_e$ and $\sigma_h = n_h e\mu_h$ are the electron and hole conductivity, respectively. For high B, we can deduce that $\Delta\rho \sim \frac{\mu_e^2\mu_h^2B^2}{\sigma_e\mu_h^2+\sigma_h\mu_e^2}$. Namely, the high mobility can solely induce a large $\Delta\rho$. This is a natural result, given that $MoTe_2$ is a typical XMR (extremely large MR) material. The increasing temperature will reduce the mobility and $\Delta\rho$. Conversely, the high mobility at low temperatures will naturally give rise to a resistivity plateau, as observed in Ref. 20, which is actually the rediscovery of the XMR.[25]

A related question is the B-dependence at different temperatures. In Ref. 20, it is suggested that the power exponent approaches 2 at high temperature and diverges from 2 at low temperature. This is easy to understand in the framework of normal MR. Pippard has demonstrated that the MR shows varying dependence for different scales of $\omega_c\tau$, i.e., μB.[30] The MR follows quadratic dependence in the low limit of μB, and approaches saturation in the high limit of μB, and runs linearly in the intermediate region. Since the low temperature always indicates a larger mobility, the observation in Ref. 20 can be explained. Such an evolution should not involve with chiral anomaly.

IV. CONCLUSIONS

In summary, the angular dependence of PHE and AMR is studied in detail for the type-II WSM T_d-$MoTe_2$. We demonstrate that the anisotropic resistivity $\Delta\rho$ arises from the OMR that increases the $\rho_{\perp}$ more quickly, instead of the reduced $\rho_{\parallel}$ as expected in the chiral anomaly effect. In contrast, the positive LMR indicates that the large OMR dominates over the chiral anomaly effect. This explains why it is difficult to measure NLMR in type-II WSMs. We argue that the measured PHE can be related with the chiral anomaly only when the NLMR is simultaneously observed.

ACKNOWLEDGMENTS

This work was supported by the National Key R&D Program of China (Grant Nos. 2016YFA0300404, 2017YFA0403600 and 2017YFA0403502), the National Natural Science Foundation of China (Grant Nos. U1532267, 11674327, 11874363, 51603207, 11574288 and U1732273).

REFERENCES

[1] X. G. Wan, A. M. Turner, A. Vishwanath, and S. Y. Savrasov, Phys. Rev. B **83**, 205101 (2011).
[2] A. A. Soluyanov, D. Gresch, Z. Wang, Q. Wu, M. Troyer, X. Dai, and B. A. Bernevig, Nature **527**, 495 (2015).
[3] Y. Sun, S.-C. Wu, M. N. Ali, C. Felser, and B. Yan, Phys. Rev. B **92**, 161107 (2015).
[4] Y. Wu, D. Mou, N. H. Jo, K. Sun, L. Huang, S. L. Bud'ko, P. C. Canfield, and A. Kaminski, Phys. Rev. B **94**, 121113 (2016).
[5] C. Wang, Y. Zhang, J. Huang, S. Nie, G. Liu, A. Liang, Y. Zhang, B. Shen, J. Liu, C. Hu, Y. Ding, D. Liu, Y. Hu, S. He, L. Zhao, L. Yu, J. Hu, J. Wei, Z. Mao, Y. Shi, X. Jia, F. Zhang, S. Zhang, F. Yang, Z. Wang, Q. Peng, H. Weng, X. Dai, Z. Fang, Z. Xu, C. Chen, and X. J. Zhou, Phys. Rev. B **94**, 241119 (2016).
[6] A. Tamai, Q. S. Wu, I. Cucchi, F. Y. Bruno, S. Riccò, T. K. Kim, M. Hoesch, C. Barreteau, E. Giannini, C. Besnard, A. A. Soluyanov, and F. Baumberger, Phys. Rev. X **6**, 031021 (2016).
[7] K. Deng, G. Wan, P. Deng, K. Zhang, S. Ding, E. Wang, M. Yan, H. Huang, H. Zhang, Z. Xu, J. Denlinger, A. Fedorov, H. Yang, W. Duan, H. Yao, Y. Wu, S. Fan, H. Zhang, X. Chen, and S. Zhou, Nat. Phys. **12**, 1105 (2016).
[8] H. B. Nielsen and M. Ninomiya, Phys. Lett. **130**, 389 (1983).
[9] D. T. Son and B. Z. Spivak, Phys. Rev. B **88**, 104412 (2013).
[10] Y. Wang, E. Liu, H. Liu, Y. Pan, L. Zhang, J. Zeng, Y. Fu, M. Wang, K. Xu, Z. Huang, Z. Wang, H. Z. Lu, D. Xing, B. Wang, X. Wan, and F. Miao, Nat. Commun. **7**, 13142 (2016).
[11] Y. Y. Lv, X. Li, B. B. Zhang, W. Y. Deng, S. H. Yao, Y. B. Chen, J. Zhou, S. T. Zhang, M. H. Lu, L. Zhang, M. Tian, L. Sheng, and Y. F. Chen, Phys. Rev. Lett. **118**, 096603 (2017).
[12] A. A. Burkov, Phys. Rev. B **96**, 041110 (2017).
[13] S. Nandy, G. Sharma, A. Taraphder, and S. Tewari, Phys. Rev. Lett. **119**, 176804 (2017).
[14] N. Kumar, S. N. Guin, C. Felser, and C. Shekhar, Phys. Rev. B **98**, 041103 (2018).

[15]H. Li, H.-W. Wang, H. He, J. Wang, and S.-Q. Shen, Phys. Rev. B **97**, 201110 (2018).
[16]S. Liang, J. Lin, S. Kushwaha, J. Xing, N. Ni, R. J. Cava, and N. P. Ong, Phys. Rev. X **8**, 031002 (2018).
[17]Y. J. Wang, J. X. Gong, D. D. Liang, M. Ge, J. R. Wang, W. K. Zhu, and C. J. Zhang, preprint arXiv:1801.05929.
[18]P. Li, C. H. Zhang, J. W. Zhang, Y. Wen, and X. X. Zhang, Phys. Rev. B **98**, 121108 (2018).
[19]J. Yang, W. L. Zhen, D. D. Liang, Y. J. Wang, X. Yan, S. R. Weng, J. R. Wang, W. Tong, L. Pi, W. K. Zhu, and C. J. Zhang, Phys. Rev. Materials **3**, 014201 (2019).
[20]F. C. Chen, X. Luo, J. Yan, Y. Sun, H. Y. Lv, W. J. Lu, C. Y. Xi, P. Tong, Z. G. Sheng, X. B. Zhu, W. H. Song, and Y. P. Sun, Phys. Rev. B **98**, 041114 (2018).
[21]R. Singha, S. Roy, A. Pariari, B. Satpati, and P. Mandal, Phys. Rev. B **98**, 081103 (2018).
[22]H. X. Tang, R. K. Kawakami, D. D. Awschalom, and M. L. Roukes, Phys. Rev. Lett. **90**, 107201 (2003).
[23]A. Fernández-Pacheco, J. M. De Teresa, J. Orna, L. Morellon, P. A. Algarabel, J. A. Pardo, M. R. Ibarra, C. Magen, and E. Snoeck, Phys. Rev. B **78**, 212402 (2008).
[24]A. A. Taskin, H. F. Legg, F. Yang, S. Sasaki, Y. Kanai, K. Matsumoto, A. Rosch, and Y. Ando, Nat. Commun. **8**, 1340 (2017).
[25]F. C. Chen, H. Y. Lv, X. Luo, W. J. Lu, Q. L. Pei, G. T. Lin, Y. Y. Han, X. B. Zhu, W. H. Song, and Y. P. Sun, Phys. Rev. B **94**, 235154 (2016).
[26]T. Zandt, H. Dwelk, C. Janowitz, and R. Manzke, J. Alloys Compd. **442**, 216 (2007).
[27]J. X. Gong, J. Yang, M. Ge, Y. J. Wang, D. D. Liang, L. Luo, X. Yan, W. L. Zhen, S. R. Weng, L. Pi, C. J. Zhang, and W. K. Zhu, Chin. Phys. Lett. **35**, 097101 (2018).
[28]T. Liang, Q. Gibson, M. N. Ali, M. Liu, R. J. Cava, and N. P. Ong, Nat. Mater. **14**, 280 (2015).
[29]X. Huang, L. Zhao, Y. Long, P. Wang, D. Chen, Z. Yang, H. Liang, M. Xue, H. Weng, Z. Fang, X. Dai, and G. Chen, Phys. Rev. X **5**, 031023 (2015).
[30]A. B. Pippard, *Magnetoresistance in metals* (Cambridge University Press, Cambridge, 1989).
[31]S. Nandy, A. Taraphder, and S. Tewari, Sci. Rep. **8**, 14983 (2018).